JCIM JOURNAL OF CHEMICAL INFORMATION AND MODELING

pubs.acs.org/jcim Article

Targeting the Receptor-Binding Motif of SARS-CoV-2 with D-Peptides Mimicking the ACE2 Binding Helix: Lessons for Inhibiting Omicron and Future Variants of Concern

Pedro A. Valiente, Satra Nim, JinAh Lee, Seungtaek Kim, and Philip M. Kim*

Cite This: J. Chem. Inf. Model. 2022, 62, 3618−3626 Read Online

ACCESS | Metrics & More | Article Recommendations | Supporting Information

ABSTRACT: The COVID-19 pandemic continues to spread around the world, with several new variants emerging, particularly those of concern (VOCs). Omicron (B.1.1.529), a recent VOC with many mutations in the spike protein's receptor-binding domain (RBD), has attracted a great deal of scientific and public interest. We previously developed two D-peptide inhibitors for the infection of the original SARS-CoV-2 and its VOCs, alpha and beta, *in vitro*. Here, we demonstrated that Covid3 and Covid_extended_1 maintained their high-affinity binding (29.4−31.3 nM) to the omicron RBD. Both D-peptides blocked the omicron variant *in vitro* infection with IC50s of 3.13 and 5.56 μM, respectively. We predicted that Covid3 shares a larger overlapping binding region with the ACE2 binding motif than different classes of neutralizing monoclonal antibodies. We envisioned the design of D-peptide inhibitors targeting the receptor-binding motif as the most promising approach for inhibiting current and future VOCs of SARS-CoV-2, given that the ACE2 binding interface is more limited to tolerate mutations than most of the RBD's surface.

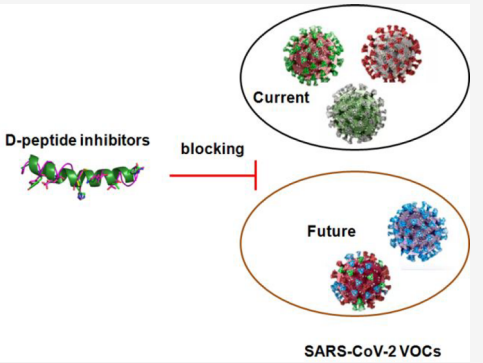

INTRODUCTION

Blocking the RBD-ACE2 association is a therapeutic or prophylactic approach for preventing SARS-CoV-2 infection.[1−4] However, due to the ongoing global spreading, SARS-CoV-2 continues to evolve into new variants of concern (VOCs) such as the alpha (B.1.1.7), beta (B.1.1.351), gamma (P1), delta (B.1.1.617.2), and omicron (B.1.1.529).[5,6] Unlike other VOCs that evolved while natural immunity was dominant, omicron's emergence after vaccination against SARS-CoV-2 was significant.[7]

The omicron variant has become prevalent worldwide, exhibiting an improved transmission and immunoescape.[7] Omicron has an unprecedented high number of mutations when compared to the original strain of SARS-CoV-2, particularly in the spike protein (37 mutations) and its RBD (15 substitutions),[8] the target region of most Covid-19 vaccines and therapeutic antibodies. Recent studies have revealed that omicron has a significant level of escape from known neutralizing monoclonal antibodies,[9,10] and sera from convalescent patients,[11] or individuals immunized with the Pfizer vaccine BNT162b2[12] even after a booster dose.[10,13]

Few therapeutic monoclonal antibodies maintained fully or partially their neutralizing activity against omicron;[8,10] but unfortunately, antibodies have drawbacks for intranasal delivery, and also they are costly, making them inappropriate candidates for large-scale treatments or use in poor economies. D-Peptides have clear benefits for therapeutic applications, including low antigenicity, relatively low cost, and elevated-protease stability.

Recently, we developed two D-peptide inhibitors for the infection of the original SARS-CoV-2 and its VOCs alpha (B.1.1.7) and beta (B.1.1.351).[3] Here, we showed both peptides maintained their high-affinity binding (29.4−31.3 nM) to the omicron RBD. Covid3 and Covid_extended_1 blocked the omicron variant *in vitro* infection with IC50s of 3.13 and 5.56 μM, respectively. Both D-peptides target the ACE2 binding motif and emerge as a promising suitable treatment to neutralize the infection of current and future VOCs of SARS-CoV-2.

MATERIALS AND METHODS

Molecular Dynamics Simulations. The GROMACS software package[14] version 2019.3 was used to perform the molecular dynamics (MD) simulations of the omicron RBD +Covid3 complex using the CHARMM36-m force field[15] and the TIP3P water model.[16] The omicron RBD+Covid3 complex was solvated in an octahedron box with ∼16278 water

Received: April 26, 2022
Published: July 24, 2022

https://doi.org/10.1021/acs.jcim.2c00500
J. Chem. Inf. Model. 2022, 62, 3618−3626

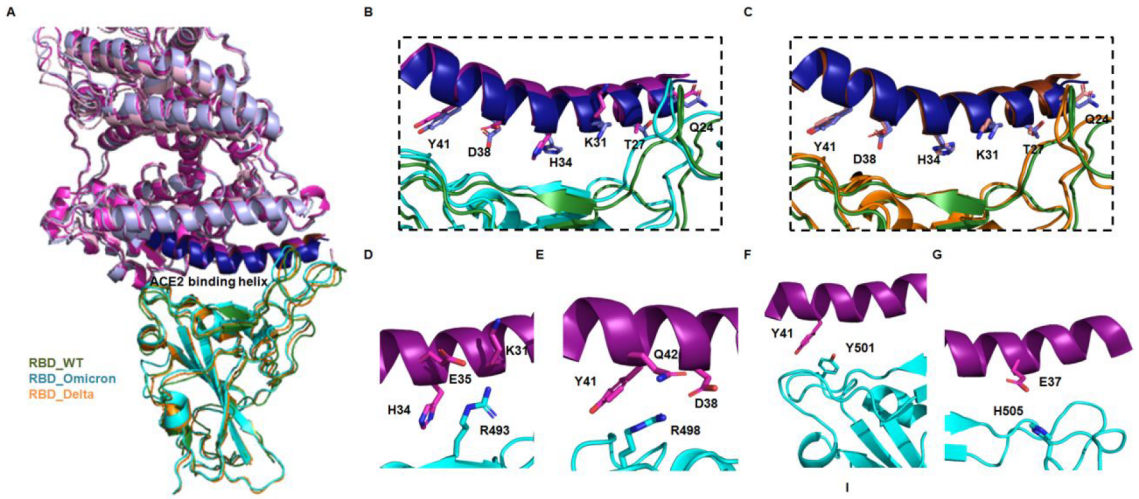

Figure 1. Key hotspots in the ACE2 binding helix share a similar binding mode with the original and omicron RBD. **A**) Structural superposition of the X-ray structures of the complexes of the **ACE2+RBD_WT** (RBD (green); ACE2 binding helix (dark blue); rest of the ACE2 (light blue); pdb code: 6m17), **ACE2+RBD_Delta** (RBD (orange); ACE2 binding helix (dark brown); rest of the ACE2 (light brown); pdb code: 7wbq), and **ACE2+RBD_Omicron** (RBD (cyan); ACE2 binding helix (dark magenta); rest of the ACE2 (light magenta); pdb code: 7wbp). **B**) Key hotspots of the ACE2 binding helix share similar side chain conformations when bound to original (dark blue) and omicron (dark magenta) RBD. **C**) Key hotspots of the ACE2 binding helix share similar side chain conformations when bound to original (dark blue) and delta (dark brown) RBD. **D**) Zoom of the interaction of R493 with the ACE2 binding helix. **E**) Zoom of the interaction of R498 with the ACE2 binding helix. **F**) Zoom of the interaction of Y501 with the ACE2 binding helix. **G**) Zoom of the interaction of H505 with the ACE2 binding helix.

molecules. To ensure the system electroneutrality, sufficient Na^+Cl^- counterions were added to the solvation box. Two consecutive energy minimization (EM) schemes were used to relax the systems. Then, the systems were heated in the NVT ensemble before being equilibrated in the NPT ensemble at p = 1 bar and T = 310 K. In both steps, we progressively released the position restraints that were applied to the protein heavy atoms. Finally, the production NPT runs were performed by duplicating for 200 ns. The EM and MD simulations were set up similarly to previous works.[3,17]

The GROMACS software package[14] version 2019.3 was used for all trajectory analyses. The most representative structure sampled along the MD simulations was calculated over the complex heavy atoms with the GROMOS algorithm[18] implemented in the gmx cluster program,[14] using an rmsd cutoff value of 0.15 nm.

Free Energy Calculations Using the Crooks Gaussian Intersection Method. To predict the effect of different point mutations in the omicron RBD on the D-peptides' binding affinity, we used the Crooks Gaussian Intersection (CGI) method with the dual system single-box approximation. Briefly, in the dual system single-box setup, a wild-type RBD bound to a D-peptide is placed in the same box with a solvated unbound mutant RBD (λ = 0). The other end-state (λ = 1) contains a mutant RBD bound to a D-peptide with a solvated wild-type RBD (Figure S1).[19] Position restraints were applied at the backbone atoms of the RBD's Val32 to prevent the interaction between the solvated RBD and the RBD+peptide complex due to translation and rotation movements during the MD simulation. The pmx package was used to generate the simulation topologies and input files for the CHARMM36-m force field.[15,20] Equilibrium MD simulations of 100 ns length were performed for each state (λ = 0 and λ = 1) using the previously described simulation parameters.[20] From each simulation, the first 10 ns were discarded, snapshots were picked every 400 ps, and short nonequilibrium thermodynamic integration runs (500 ps) were conducted in which λ was switched from 0 to 1 or from 1 to 0, respectively. The derivative of the Hamiltonian with respect to λ was computed at each step, and the binding free energy difference for the transformation was estimated following Goette and Grübmueller.[21] The binding free energy calculated corresponds to a double free energy difference: $\Delta\Delta G = \Delta G_4 - \Delta G_3$ (Figure S1).

Peptide Synthesis. Lifetein LLC produced, purified, and characterized the Covid3 and Covid_extended_1 D-peptides. A brief description of the synthesis protocol provided by the supplier can be found in our previous study.[3] The purity of both peptides exceeds 95%. We provided detailed information about the characterization of these peptides in the Supporting Information (weight, molecular weight, purity, HPLC, and MS) (Table S1 and Figures S2−S5).

D-Peptide BLI Measurements. BLI measurements were conducted using the ForteBio Octet RED96 instrument and biosensors. ForteBio Data Analysis 9.0 software was used for data analysis. Kinetics experiments were performed at 25 °C with a sample plate shake speed of 1000 rpm and the Standard Kinetics Acquisition rate (5.0 Hz, averaging by 20).

Acrobiosystems provided the His-tagged omicron RBD and human ACE2 purified proteins. His-tagged omicron RBD purified protein was loaded onto Ni-NTA sensors at a concentration of 200 nM. Peptides were loaded at different concentrations to the bound sensors. The dissociation step was measured by dipping bound sensors back into the wells used to acquire the baseline time progression. As controls, nonspecific His-tagged SUMO protein and His-tagged RBD loaded alone were used to deduct binding due to nonspecific interactions of the peptides with the sensors. The values of the kinetics and thermodynamics parameters ka, kd, and K_d were calculated using the subtracted binding curves.

Virus Neutralization Assays. The SARS-CoV-2 B.1.529 (hCoV-19/Korea/KDCA447321/2021) isolate was obtained

https://doi.org/10.1021/acs.jcim.2c00500
J. Chem. Inf. Model. 2022, 62, 3618−3626

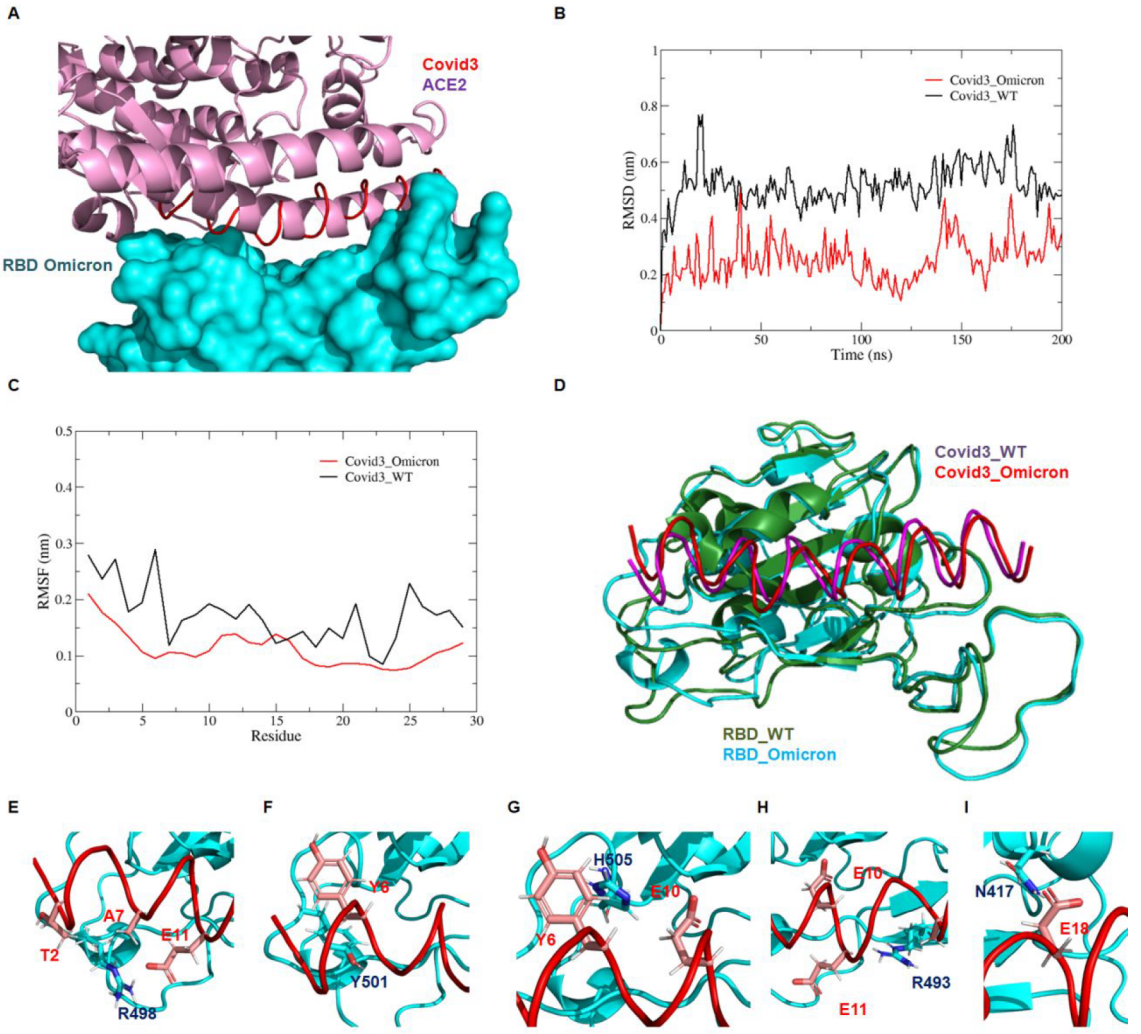

Figure 2. Three-dimensional modeling of the omicron RBD-Covid3 complex. **A**) 3D structure of Covid3 superimposed over the omicron RBD (magenta, cartoon) coupled with the ACE2 receptor (cyan, surface). In red, is displayed Covid3. **B**) Root mean square deviation (RMSD) of the heavy atoms of Covid3 bound to the wild-type and omicron RBDs. **C**) Root mean square fluctuation (RMSF) per residue of Covid3 bound to the wild-type and omicron RBDs. **D**) Structural superimposition of the most representative cluster structures extracted from the MD simulation of Covid3 coupled to the wild-type and omicron RBDs. **E**) Zoom of the Covid3's binding contact residues with R498. **F**) Zoom of the Covid3's binding contact residues with Y501. **G**) Zoom of the Covid3's binding contact residues with H505. **H**) Zoom of the Covid3's binding contact residues with R493. **I**) Zoom of the Covid3's binding contact residues with N417.

from the Korea Disease Control and Prevention Agency. This lineage was expanded in Vero E6 cells (ATCC CRL-1586) in Dulbecco's Modified Eagle's Medium (DMEM, Welgene, Gyeongsan, Republic of Korea) with 2% fetal bovine serum (Gibco, Thermo Scientific, Waltham, MA, USA). The cells were seeded in T-175 flasks, infected with the omicron variant, and incubated at 37 °C in 5% CO_2. The viruses were collected 3 days after infection and kept at −80 °C. The virus neutralization experiments were conducted as described earlier.[22] Briefly, Vero E6 cells were grown in 96-well plates (0.5×10^4 cells/well) in Opti-PRO SFM (Thermo Scientific, Waltham, MA, USA) supplied with 4 mM L-glutamine and 1× Antibiotics-Antimycotic (Thermo Scientific, Waltham, MA, USA) and propagated for 24 h at 37 °C in 5% CO_2. Peptides were solubilized in 100% dimethyl sulfoxide (DMSO, Sigma-Aldrich, St. Louis, MO, USA) and diluted in phosphate buffered saline (PBS, Welgene, Gyeongsan, Republic of Korea) at concentrations ranging from 100 μM to 0.1953 μM. 2-fold serially diluted peptides were added to 500 $TCID_{50}$ of the omicron variant and preincubated for 30 min at 37 °C. Then, the mix was incubated with the Vero E6 cells and propagated for 6 days at 37 °C in 5% CO_2. The cytopathic effect (CPE) in each well was observed following crystal violet staining 4 days after infection. The dose−response inhibition equation implemented in the GraphPad Prism 6 software (GraphPad Software, La Jolla, CA, USA) was used to determine the IC_{50} values. As a positive control of the virus neutralization experiments, we included the first international standard for anti-SARS-CoV-2 immunoglobulin (NIBSC code 20/136). As a negative control, we used PBS (data not shown). In the Supporting Information, we displayed the % of virus inhibition, for the control, as a function of the dilution ratio.

RESULTS

SARS-CoV-2 D-Peptide Inhibitors Maintain Their High-Affinity Binding to the Omicron's RBD. A recent study showed the omicron RBD-ACE2 and delta RBD-ACE2 crystal structures have a similar overall conformation with the

https://doi.org/10.1021/acs.jcim.2c00500
J. Chem. Inf. Model. 2022, 62, 3618−3626

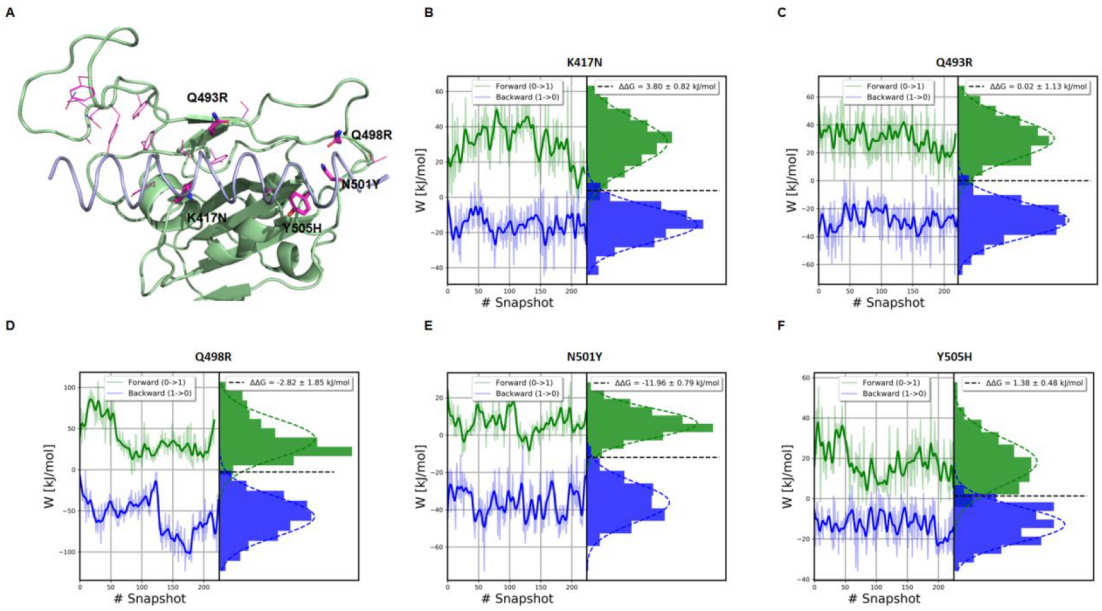

Figure 3. Predicting the impact of mutations in the binding interface over the affinity of Covid3 by the wild-type RBD. **A**) Mapping mutations within the binding interface of Covid3 and the omicron RBD. **B**) K417N, **C**) Q493R, **D**) Q498R, **E**) N501Y, and **F**) Y505H. The CGI method was used to calculate the binding free energy differences using the dual system single-box approach. Panels B and E are adapted from ref 3.

original RBD-ACE2 structure (Figure 1A).[7] Here, we showed that except for K31, all the other critical hotspots in the ACE2 binding helix share a similar conformation when bound to the RBD from the original, delta, and omicron variants (Figure 1B,C). Notably, critical ACE2 hotspots like H34, D38, and Y41 strongly interact with relevant positions mutated within the omicron receptor binding motif (RBM), R493, R498, and Y501, respectively, while E35 and E37, two residues not previously selected as hotspots to develop our D-analogs, bind to R493 and H505, respectively (Figure 1D−G). Thus, we reasoned that our previous D-peptide designs could bind the omicron's RBD with potency similar to the original's RBD.

In the second step, we superimposed the D-peptide structure into the omicron RBD-ACE2 X-ray structure to model the 3D structure of the complex between the omicron's RBD and Covid3 (7wbp, Figure 2A). We then assessed the stability of the omicron RBD+Covid3 complex through MD simulations of 200 ns. As a control, we also simulated the wild-type RBD bound to Covid3. Similar to our past study, no glycosylations were added to the RBD structure (segment N331-E516) for running the MD simulations.[3] This structure region lacks two key N-glycosylation sites for changing the RBD's conformational dynamics: N165 and N234.[23] As in our previous study, no glycans were modeled at positions N331 and N343 since they are too far from the RBD's D-peptide binding site.[3] The RMSD and RMSF profiles calculated for the Covid3's heavy atoms all through the MD simulations revealed that the peptide bound to the omicron RBD was more stable than the one coupled to the wild-type RBD (Figure 2B,C, Figure S6). Most of the residues had RMSF values between 0.1 and 0.2 nm indicating that Covid3 was stable when bound to the omicron RBD. The superposition of the most representative structures obtained from the MD simulations disclosed that Covid3 targets a similar binding region in both RBDs (Figure 2D). Following that, we analyze the binding interface of the omicron RBD+Covid3 complex to understand the molecular interactions that keep the peptide's affinity by omicron. Our predictions revealed that the RBD mutated positions Q498R and N501Y directly interacted with residues E11 and Y6 of Covid3, respectively (Figure 2E,F). Both residues of the D-peptide keep critical interactions established by the hotspots E38 and Y41 in the X-ray structure of the omicron RBD+ACE2 complex (Figure 1E,F). For mutation Y505H, the detrimental effect of losing the stacking contact with Y6 seems to be partially compensated by interacting with E10 of Covid3 (Figure 2G). The lack of relevant interactions of R493 suggests a negligible impact of mutation N493R on the D-peptide's affinity. Lastly, the close contact between N417 and the residue E18 of Covid3 supports our previous prediction about the low impact of mutation K417N on the D-peptide's affinity by the RBD.[3]

Next, we evaluated *in silico* the influence of different point mutations on the strength of our D-peptides for associating with the omicron's RBD using as the starting point our previous model of the wild-type RBD in complex with the D-peptide Covid3.[3] According to our structural analysis, only the mutations K417N, Q493R, Q498R, N501Y, and Y505H were found within the RBD's binding interface (Figure 3A). Previously, we calculated the effect of K417N ($\Delta\Delta G$ = 3.80 ± 0.82 kJ/mol) and N501Y ($\Delta\Delta G$ = −11.96 ± 0.79 kJ/mol) over the D-peptides' binding affinity.[3] These mutations were located on the ACE2 binding interface of the alpha (N501Y) and beta (N501Y and K417N) RBDs (Figure 3B,E).[7] Following that, we used the Crooks Gaussian Intersection (CGI) approach to estimate how much the point mutations Q493R, Q498R, and Y505H will hinder our designs to target the omicron's RBD. The free energy calculations indicated that mutation Q498R ($\Delta\Delta G$ = −2.82 ± 1.85 kJ/mol) must slightly increase the affinity of Covid3, while the change Q493R (0.02 ± 1.13 kJ/mol) might be negligible over the binding (Figure 3C,D). In comparison, mutation Y505H (1.38 ± 0.48 kJ/mol) could have a small negative effect over the D-peptide's binding affinity (Figure 3F). Overall, the cumulative impact of these

https://doi.org/10.1021/acs.jcim.2c00500
J. Chem. Inf. Model. 2022, 62, 3618−3626

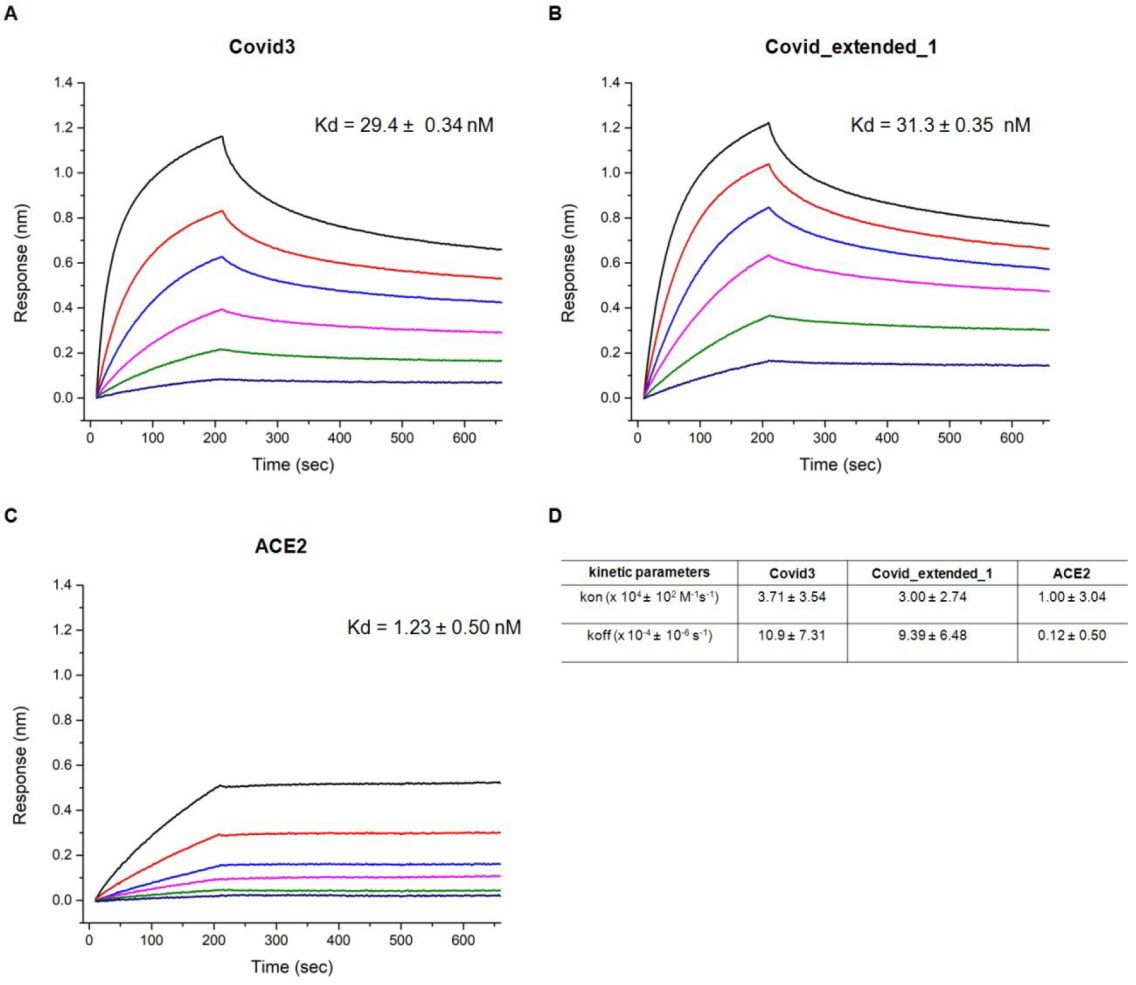

Figure 4. The design D-peptides are high affinity binders of the omicron RBD. **A**) Biolayer interferometry assays were used to measure the Covid3 binding affinity to the omicron RBD (K_d = 29.4 ± 0.34 nM). **B**) Biolayer interferometry assays were used to measure the Covid_extended_1 binding affinity to the omicron RBD (K_d = 31.3 ± 0.35 nM). **C**) Biolayer interferometry assays were used to measure the ACE2 binding affinity to the omicron RBD (K_d = 1.23 ± 0.50 nM). The concentrations of Covid3, Covid_extended_1, and ACE2 loaded to the sensors were displayed using different line colors: as black (1 μM), red (0.5 μM), blue (0.25 μM), magenta (0.125 μM), green (0.063 μM), and dark blue (0.031 μM). **D**) Summary of the determined kinetic parameters for the direct binding of Covid3, Covid_extended_1, and ACE2 with the omicron RBD.

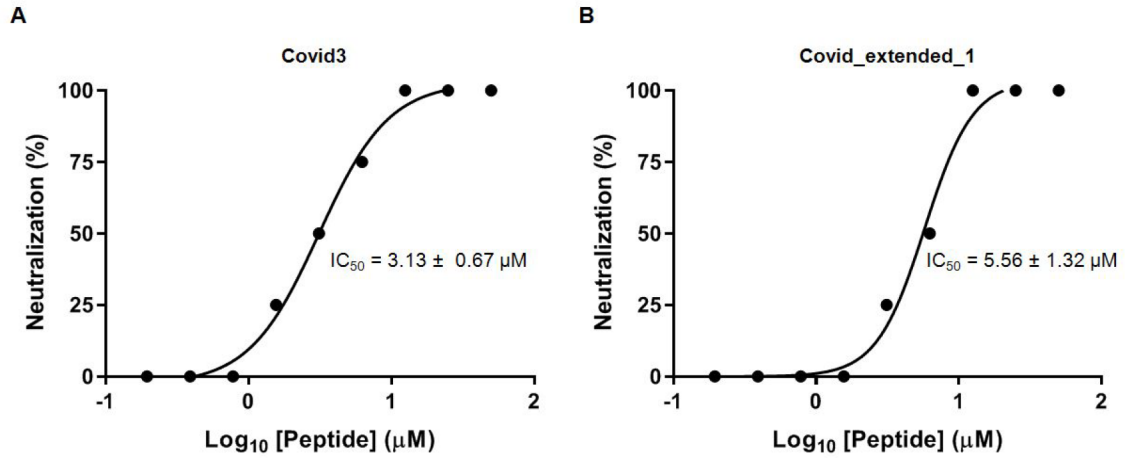

Figure 5. Covid3 and Covid_extended_1 blocked the omicron SARS-CoV-2 infection in Vero E6 cells. **A**) Covid3 blocked the omicron infection with an IC50 of 3.13 ± 0.67 μM. **B**) Covid_extended_1 blocked the omicron infection with an IC50 of 5.56 ± 1.32 μM. Before being incubated with Vero E6 cells, different concentrations of Covid3 and Covid_extended_1 were mixed with 500 $TCID_{50}$ of the omicron variant.

https://doi.org/10.1021/acs.jcim.2c00500
J. Chem. Inf. Model. 2022, 62, 3618−3626

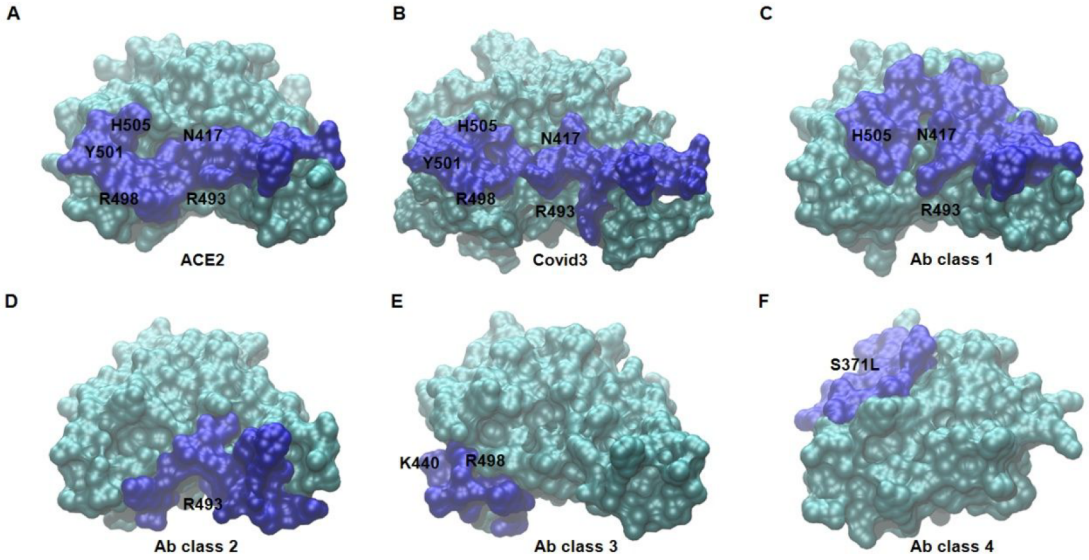

Figure 6. Mapping the omicron RBD binding interface of the human ACE2, Covid3, and different groups of neutralizing monoclonal antibodies. The omicron RBD binding interface is colored in blue, while the rest of the RBD is colored in cyan. **A**) Human ACE2 (pdb code: 7wbp). **B**) Covid3. **C**) Ab class 1 (CB6, 7c01). **D**) Ab class 2 (LY-CoV555, 7kmg). **E**) Ab class 3 (REGN10987, 6xdg). **F**) Ab class 4 (S2X259, 7ral). Mutations within the omicron RBD binding interface are also mapped.

point mutations should not reduce the binding strength of Covid3 by the omicron's RBD.

Then, we evaluated how Covid3 and Covid_extended_1 could directly bind the omicron RBD using biolayer interferometry (BLI) assays. Ni-NTA (nitrilotriacetic acid) biosensors were used to properly immobilize His-tagged omicron RBD and test both D-peptides' direct coupling. We observed that both D-peptides had similar affinities for binding the omicron RBD. Kinetic fits reveal that Covid3 has the highest affinity (29.4 ± 0.34 nM) for the omicron RBD, followed by Covid_extended_1 (31.3 ± 0.35 nM) (Figure 4A,B). We also evaluated the dissociation constant of the omicron RBD-ACE2 complex (K_d = 1.23 ± 0.50 nM) as a positive control (Figure 4C). A summary of the kinetic parameters for the direct binding of these molecules with the omicron RBD is also shown (Figure 4D).

The D-Peptide Inhibitors Kept Their Neutralizing Activity against Omicron. Finally, we tested the efficacy of Covid3 and Covid_extended_1 to prevent the omicron infection of Vero E6 cells. Before being incubated in Vero E6 monolayers, different concentrations of both peptides were mixed with 500 TCID50 of the omicron variant. Covid3 and Covid_extended_1 inhibited the infection of omicron with IC50s of 3.13 ± 0.67 μM and 5.56 ± 1.32 μM, respectively (Figure 5). In a previous study, we confirmed neither peptide is toxic for Vero E6 cells in the concentration ranges evaluated in the virus neutralization experiments.[3] As a positive control, we used the first anti-SARS-CoV-2 immunoglobulin international standard (NIBSC code 20/136) (Figure S7).

Covid3 Shares a Larger Overlapping Binding Region with the ACE2 Binding Motif than Different Classes of Neutralizing Monoclonal Antibodies. We compared the binding region targeted by the ACE2 and Covid3 with those previously mapped for four different classes of monoclonal antibodies that fail to neutralize the omicron variant (Figure 6). We also mapped omicron's immunoescape mutations within the binding interface of each complex. To run our comparisons, we selected etesevimab (CB6)[1] as an example of class 1, bamlanivimab (LY-CoV555)[24] as an example of class 2, imdevimab (REGN10987)[25] as an example of class 3, and S2X259[26] as an example of class 4. Monoclonal antibodies of classes 1 and 2 compete for binding to the human ACE2, whereas monoclonal antibodies from classes 3 and 4 bind away from the human ACE2 binding motif (Figure 6C−F). Significantly, Covid3 shares a larger overlapping binding region with the ACE2 than the monoclonal antibodies from classes 1 and 2.

DISCUSSION

The molecular targeting of the RBD-ACE2 interaction by high-affinity binders is a widely used strategy for inhibiting SARS-CoV-2 infection. Numerous neutralizing molecules have been described for the original SARS-CoV-2 variant, including soluble and modified ACE2,[2728] linear peptides,[29] antibodies,[1,2,30,31] and *de novo* design proteins.[32] However, the omicron variant escapes the vast majority of current SARS-CoV-2 neutralizing antibodies.[6,9,10] Recently, we developed two D-peptide inhibitors for the infection of the original SARS-CoV-2 and its VOCs alpha and beta *in vitro*.[3] Here, we reported that Covid3 and Covid_extended_1 bind the omicron RBD with a dissociation constant (K_d) of 29.4 and 31.3 nM, respectively. Both D-peptides maintain an affinity for the omicron RBD similar to the one previously reported for the wild-type RBD.[3] MD simulations predicted a more stable binding mode for Covid3 when coupled to the omicron RBD than when bound to the wild-type RBD. Notably, Covid3 targets a similar binding region in both RBDs. We also predicted the central role of mutation N501Y in maintaining the D-peptides' high affinity for the omicron RBD. Large-scale mutagenesis studies on the RBD ACE2 binding motif corroborated our prediction, indicating that mutations reducing the polar character at N501 can improve the affinity.[33]

Both D-peptide inhibitors have a lesser affinity (K_d = 29−31 nM) for the omicron RBD than several miniproteins previously reported with K_d values in the pM range.[32,34] We showed that

https://doi.org/10.1021/acs.jcim.2c00500
J. Chem. Inf. Model. 2022, 62, 3618−3626

both D-peptide blockers dissociate at similar rates as these miniproteins.[34] Then, our D-peptide designs have lower affinity than these miniprotein blockers due to their reduced association rates. Remarkably, Covid3 and Covid_extended_1 neutralized the omicron infection of Vero E6 cells with IC50s of 3.13 ± 0.67 μM and 5.56 ± 1.32 μM, respectively. These findings revealed that both D-peptides retained the omicron-neutralizing activity exhibited against the original, alpha, and beta SARS-CoV-2 variants. As expected, both D-peptide inhibitors (IC50s = 3−5 μM) have a lower omicron-neutralizing potency on a molar basis than TRI2-2 (IC50 = 376 pM), a multivalent miniprotein inhibitor recently designed by Baker's group for targeting the RBD's ACE2 binding motif.[34] Given that these peptides have a substantially smaller molecular weight than TRI2-2, their potency per gram is much closer.

Understanding the molecular mechanism for neutralizing SARS-CoV-2 is essential for developing universal inhibitors of the present and future VOCs. We compared the omicron RBD binding interface of Covid3 with those previously mapped from different groups of neutralizing antibodies that failed to inhibit the omicron RBD-ACE2 interaction. We predicted that Covid3 almost resembles ACE2 in binding the omicron RBD. A recent study disclosed omicron's mutations conferring resistance to different classes of monoclonal antibodies: Q493R (classes 1 and 2), K417N (classes 1 and 2), N440 K (class 3), G446S (class 3), and S371L (class 4).[6] Significantly, mutations in omicron that give resistance to monoclonal antibodies of classes 3 and 4 are located outside of the D-peptide's binding interface. Other immunoescape mutations found in the VOCs beta (E484K) and delta (E484Q, L452R) conferring resistance to monoclonal antibodies of classes 2 and 3 were also mapped outside of the D-peptide's binding interface,[35] while omicron's mutations responsible for resistance to monoclonal antibodies of classes 1 and 2 are within the binding interface of the D-peptides. Of significance, the residues Y6 and E11 of Covid3 mimic critical interactions established by the ACE2 hotspots Y41 and E38 with the RBD mutated positions N501Y and N498R in the omicron RBD-ACE2 X-ray structure.[7] On the other hand, the lack of critical interactions of N493R with Covid3 suggests a poor impact of this mutation on the D-peptides' binding affinity.

Finally, we envision using D-peptide blockers mimicking the ACE2 binding helix as the most promising strategy to inhibit current and future VOCs of SARS-CoV-2. Deep mutagenesis studies showed the ACE2 binding interface is more restricted in accepting mutations than most of the RBD's surface.[33] This feature might prevent the viral escape from molecules targeting this binding motif. Further studies using animal models would be needed to evaluate our current designs' toxicity, pharmacodynamics, and pharmacokinetics in more detail.

CONCLUSIONS

Here, we showed that two D-peptides mimicking the ACE2 binding helix are nanomolar binders of the omicron RBD. Both peptides effectively retained the neutralizing activity shown for the original, alpha, and beta variants against omicron. We predicted our D-peptides target a similar binding interface at the wild-type and omicron RBDs. We visualize using these D-peptide analogs as universal inhibitors for current and future VOCs of SARS-CoV-2.

DATA AND SOFTWARE AVAILABILITY

The following is a list of software and web sites: CLICK (D-peptides superimposition), http://cospi.iiserpune.ac.in/click/Download/Click_X86_64.zip; Gromacs version 2019.3 (MD simulations), http://ftp.gromacs.org/pub/gromacs/gromacs-2019.3.tar.gz; pmx (free energy calculations setup), https://github.com/deGrootLab/pmx; Pymol 2.5 (molecular graphics generation), https://github.com/schrodinger/pymol-open-source; Graphpad Prism (BLI plots), https://www.graphpad.com/scientific-software/prism/; experimental structures, http://www.rcsb.org. Crystal structures were obtained and downloaded from the Protein Data Bank: ACE2+RBD_Omicron (pdb code: 7wbp), ACE2+RBD_Delta (7wbq), ACE2+RBD_WT (6m17), Ab class 1 (CB6, 7c01), Ab class 2 (LY-CoV555, 7kmg), Ab class 3 (REGN10987, 6xdg), Ab class 4 (S2X259, 7ral).

ASSOCIATED CONTENT

Supporting Information

The Supporting Information is available free of charge at https://pubs.acs.org/doi/10.1021/acs.jcim.2c00500.

Figure S1, CGI method used to calculate binding free energy differences using dual system single-box setup; Figure S2, HPLC report of D-peptide Covid3; Figure S3, Covid3's ESI mass spectrometry report; Figure S4, Covid_extended_1's HPLC report; Figure S5, Covid_extended_1's ESI mass spectrometry report; Figure S6, RMSD of heavy atoms of Covid3 bound to omicron RBD; Figure S7, omicron virus neutralization assay for anti-SARS-CoV-2 immunoglobulin standard as function of dilution ratio; and Table S1, both D-peptides' certificate of analysis (PDF)

PDB file (PDB)

AUTHOR INFORMATION

Corresponding Author

Philip M. Kim − *Donnelly Centre for Cellular and Biomolecular Research, Department of Molecular Genetics, and Department of Computer Science, University of Toronto, Toronto, Ontario M5S 3E1, Canada;* orcid.org/0000-0003-3683-152X; Email: pm.kim@utoronto.ca

Authors

Pedro A. Valiente − *Donnelly Centre for Cellular and Biomolecular Research, University of Toronto, Toronto, Ontario M5S 3E1, Canada;* orcid.org/0000-0002-4776-6017

Satra Nim − *Donnelly Centre for Cellular and Biomolecular Research, University of Toronto, Toronto, Ontario M5S 3E1, Canada*

JinAh Lee − *Zoonotic Virus Laboratory, Institut Pasteur Korea, Seongnam-si, Gyeonggi-do 13488, Republic of Korea*

Seungtaek Kim − *Zoonotic Virus Laboratory, Institut Pasteur Korea, Seongnam-si, Gyeonggi-do 13488, Republic of Korea*

Complete contact information is available at: https://pubs.acs.org/10.1021/acs.jcim.2c00500

Author Contributions

P.A.V. and P.M.K. conceptualized the study. Molecular dynamics simulations, free energy calculations, and computational analysis were carried out by P.A.V. Biolayer interferometry experiments were carried out by S.N. J.L. and

https://doi.org/10.1021/acs.jcim.2c00500
J. Chem. Inf. Model. 2022, 62, 3618−3626

S.K. performed virus neutralization assays. P.A.V., S.N., and P.M.K. wrote the manuscript. P.M.K. led and supervised the research.

Notes

The authors declare no competing financial interest.

■ ACKNOWLEDGMENTS

P.M.K. acknowledges funding from Project Grants #PJT-166008 and #PJT-153279 from the Canadian Institute for Health Research. S.N. acknowledges Greg Wasney from the Structural & Biophysical Core (SBC) Facility, Peter Gilgan Centre for Research & Learning & The Hospital for Sick Children for his support in the BLI experiments. S.K. acknowledges funding from the National Research Foundation of Korea (NRF-2017M3A9G6068245). The pathogen resource (NCCP43408) for this study was provided by the National Culture Collection for Pathogens of Korea.

■ ABBREVIATIONS

ACE2, angiotensin-converting enzyme 2; BLI, biolayer interferometry; CGI, Crooks Gaussian Intersection; EM, energy minimization; His-tagged, histidine tag; HPLC, high pressure liquid chromatography; ka, association rate constant; kd, dissociation rate constant; K_d, dissociation constant; MD, molecular dynamics; MS, mass spectra; Ni-NTA, nitrilotriacetic acid; NH2, amide group; PDB, protein data bank; RBD, receptor-binding domain; RBM, receptor-binding motif; RI, retro-inverse; RMSD, root mean square deviation; RMSF, root mean square fluctuation; SARS-CoV-2, severe acute respiratory syndrome coronavirus 2; VOCs, variants of concern

■ REFERENCES

(1) Shi, R.; Shan, C.; Duan, X.; Chen, Z.; Liu, P.; Song, J.; Song, T.; Bi, X.; Han, C.; Wu, L.; Gao, G.; Hu, X.; Zhang, Y.; Tong, Z.; Huang, W.; Liu, W. J.; Wu, G.; Zhang, B.; Wang, L.; Qi, J.; Feng, H.; Wang, F. S.; Wang, Q.; Gao, G. F.; Yuan, Z.; Yan, J. A Human Neutralizing Antibody Targets the Receptor-Binding Site of Sars-Cov-2. *Nature* **2020**, *584* (7819), 120−124.

(2) Wang, C.; Li, W.; Drabek, D.; Okba, N. M. A.; van Haperen, R.; Osterhaus, A.; van Kuppeveld, F. J. M.; Haagmans, B. L.; Grosveld, F.; Bosch, B. J. A Human Monoclonal Antibody Blocking Sars-Cov-2 Infection. *Nat. Commun.* **2020**, *11* (1), 2251.

(3) Valiente, P. A.; Wen, H.; Nim, S.; Lee, J.; Kim, H. J.; Kim, J.; Perez-Riba, A.; Paudel, Y. P.; Hwang, I.; Kim, K. D.; Kim, S.; Kim, P. M. Computational Design of Potent D-Peptide Inhibitors of Sars-Cov-2. *J. Med. Chem.* **2021**, *64* (20), 14955−14967.

(4) Alsoussi, W. B.; Turner, J. S.; Case, J. B.; Zhao, H.; Schmitz, A. J.; Zhou, J. Q.; Chen, R. E.; Lei, T.; Rizk, A. A.; McIntire, K. M.; Winkler, E. S.; Fox, J. M.; Kafai, N. M.; Thackray, L. B.; Hassan, A. O.; Amanat, F.; Krammer, F.; Watson, C. T.; Kleinstein, S. H.; Fremont, D. H.; Diamond, M. S.; Ellebedy, A. H. A Potently Neutralizing Antibody Protects Mice against Sars-Cov-2 Infection. *J. Immunol.* **2020**, *205* (4), 915−922.

(5) Li, J.; Lai, S.; Gao, G. F.; Shi, W. The Emergence, Genomic Diversity and Global Spread of Sars-Cov-2. *Nature* **2021**, *600* (7889), 408−418.

(6) Liu, L.; Iketani, S.; Guo, Y.; Chan, J. F.; Wang, M.; Liu, L.; Luo, Y.; Chu, H.; Huang, Y.; Nair, M. S.; Yu, J.; Chik, K. K.; Yuen, T. T.; Yoon, C.; To, K. K.; Chen, H.; Yin, M. T.; Sobieszczyk, M. E.; Huang, Y.; Wang, H. H.; Sheng, Z.; Yuen, K. Y.; Ho, D. D. Striking Antibody Evasion Manifested by the Omicron Variant of Sars-Cov-2. *Nature* **2022**, *602* (7898), 676−681.

(7) Han, P.; Li, L.; Liu, S.; Wang, Q.; Zhang, D.; Xu, Z.; Han, P.; Li, X.; Peng, Q.; Su, C.; Huang, B.; Li, D.; Zhang, R.; Tian, M.; Fu, L.; Gao, Y.; Zhao, X.; Liu, K.; Qi, J.; Gao, G. F.; Wang, P. Receptor Binding and Complex Structures of Human Ace2 to Spike Rbd from Omicron and Delta Sars-Cov-2. *Cell* **2022**, *185* (4), 630−640.e610.

(8) Yin, W.; Xu, Y.; Xu, P.; Cao, X.; Wu, C.; Gu, C.; He, X.; Wang, X.; Huang, S.; Yuan, Q.; Wu, K.; Hu, W.; Huang, Z.; Liu, J.; Wang, Z.; Jia, F.; Xia, K.; Liu, P.; Wang, X.; Song, B.; Zheng, J.; Jiang, H.; Cheng, X.; Jiang, Y.; Deng, S. J.; Xu, H. E. Structures of the Omicron Spike Trimer with Ace2 and an Anti-Omicron Antibody. *Science* **2022**, *375* (6584), 1048−1053.

(9) Cao, Y.; Wang, J.; Jian, F.; Xiao, T.; Song, W.; Yisimayi, A.; Huang, W.; Li, Q.; Wang, P.; An, R.; Wang, J.; Wang, Y.; Niu, X.; Yang, S.; Liang, H.; Sun, H.; Li, T.; Yu, Y.; Cui, Q.; Liu, S.; Yang, X.; Du, S.; Zhang, Z.; Hao, X.; Shao, F.; Jin, R.; Wang, X.; Xiao, J.; Wang, Y.; Xie, X. S. Omicron Escapes the Majority of Existing Sars-Cov-2 Neutralizing Antibodies. *Nature* **2022**, *602* (7898), 657−663.

(10) Planas, D.; Saunders, N.; Maes, P.; Guivel-Benhassine, F.; Planchais, C.; Buchrieser, J.; Bolland, W. H.; Porrot, F.; Staropoli, I.; Lemoine, F.; Péré, H.; Veyer, D.; Puech, J.; Rodary, J.; Baele, G.; Dellicour, S.; Raymenants, J.; Gorissen, S.; Geenen, C.; Vanmechelen, B.; Wawina-Bokalanga, T.; Martí-Carreras, J.; Cuypers, L.; Sève, A.; Hocqueloux, L.; Prazuck, T.; Rey, F. A.; Simon-Loriere, E.; Bruel, T.; Mouquet, H.; André, E.; Schwartz, O. Considerable Escape of Sars-Cov-2 Omicron to Antibody Neutralization. *Nature* **2022**, *602* (7898), 671−675.

(11) Zhang, L.; Li, Q.; Liang, Z.; Li, T.; Liu, S.; Cui, Q.; Nie, J.; Wu, Q.; Qu, X.; Huang, W.; Wang, Y. The Significant Immune Escape of Pseudotyped Sars-Cov-2 Variant Omicron. *Emerging Microbes Infect.* **2022**, *11* (1), 1−5.

(12) Cele, S.; Jackson, L.; Khoury, D. S.; Khan, K.; Moyo-Gwete, T.; Tegally, H.; San, J. E.; Cromer, D.; Scheepers, C.; Amoako, D. G.; Karim, F.; Bernstein, M.; Lustig, G.; Archary, D.; Smith, M.; Ganga, Y.; Jule, Z.; Reedoy, K.; Hwa, S.-H.; Giandhari, J.; Blackburn, J. M.; Gosnell, B. I.; Abdool Karim, S. S.; Hanekom, W.; Davies, M.-A.; Hsiao, M.; Martin, D.; Mlisana, K.; Wibmer, C. K.; Williamson, C.; York, D.; Harrichandparsad, R.; Herbst, K.; Jeena, P.; Khoza, T.; Kløverpris, H.; Leslie, A.; Madansein, R.; Magula, N.; Manickchund, N.; Marakalala, M.; Mazibuko, M.; Moshabela, M.; Mthabela, N.; Naidoo, K.; Ndhlovu, Z.; Ndung'u, T.; Ngcobo, N.; Nyamande, K.; Patel, V.; Smit, T.; Steyn, A.; Wong, E.; von Gottberg, A.; Bhiman, J. N.; Lessells, R. J.; Moosa, M.-Y. S.; Davenport, M. P.; de Oliveira, T.; Moore, P. L.; Sigal, A.; Ngs, S. A.; Team, C.-K. Omicron Extensively but Incompletely Escapes Pfizer Bnt162b2 Neutralization. *Nature* **2022**, *602* (7898), 654−656.

(13) Ai, J.; Zhang, H.; Zhang, Y.; Lin, K.; Zhang, Y.; Wu, J.; Wan, Y.; Huang, Y.; Song, J.; Fu, Z.; Wang, H.; Guo, J.; Jiang, N.; Fan, M.; Zhou, Y.; Zhao, Y.; Zhang, Q.; Liu, Q.; Lv, J.; Li, P.; Qiu, C.; Zhang, W. Omicron Variant Showed Lower Neutralizing Sensitivity Than Other Sars-Cov-2 Variants to Immune Sera Elicited by Vaccines after Boost. *Emerging Microbes Infect.* **2022**, *11* (1), 337−343.

(14) Abraham, M. J.; Murtola, T.; Schulz, R.; Páll, S.; Smith, J. C.; Hess, B.; Lindahl, E. Gromacs: High Performance Molecular Simulations through Multi-Level Parallelism from Laptops to Supercomputers. *SoftwareX* **2015**, *1−2*, 19−25.

(15) Huang, J.; Rauscher, S.; Nawrocki, G.; Ran, T.; Feig, M.; de Groot, B. L.; Grubmüller, H.; MacKerell, A. D. Charmm36m: An Improved Force Field for Folded and Intrinsically Disordered Proteins. *Nat. Methods* **2017**, *14* (1), 71−73.

(16) Jorgensen, W. L.; Chandrasekhar, J.; Madura, J. D.; Impey, R. W.; Klein, M. L. Comparison of Simple Potential Functions for Simulating Liquid Water. *J. Chem. Phys.* **1983**, *79* (2), 926−935.

(17) Valiente, P. A.; Becerra, D.; Kim, P. M. A Method to Calculate the Relative Binding Free Energy Differences of A-Helical Stapled Peptides. *J. Org. Chem.* **2020**, *85* (3), 1644−1651.

(18) Daura, X.; Gademann, K.; Jaun, B.; Seebach, D.; van Gunsteren, W. F.; Mark, A. E. Peptide Folding: When Simulation Meets Experiment. *Angew. Chem., Int. Ed. Engl.* **1999**, *38* (1−2), 236−240.

(19) Gapsys, V.; Michielssens, S.; Peters, J. H.; de Groot, B. L.; Leonov, H. Calculation of Binding Free Energies. In *Molecular Modeling of Proteins*; Kukol, A., Ed.; Springer: New York, 2015; pp 173−209, DOI: 10.1007/978-1-4939-1465-4_9.

https://doi.org/10.1021/acs.jcim.2c00500
J. Chem. Inf. Model. 2022, 62, 3618−3626

(20) Gapsys, V.; Michielssens, S.; Seeliger, D.; de Groot, B. L. Pmx: Automated Protein Structure and Topology Generation for Alchemical Perturbations. *J. Comput. Chem.* **2015**, *36* (5), 348−354.
(21) Goette, M.; Grubmüller, H. Accuracy and Convergence of Free Energy Differences Calculated from Nonequilibrium Switching Processes. *J. Comput. Chem.* **2009**, *30* (3), 447−456.
(22) Jiang, L.; Wang, N.; Zuo, T.; Shi, X.; Poon, K.-M. V.; Wu, Y.; Gao, F.; Li, D.; Wang, R.; Guo, J.; Fu, L.; Yuen, K.-Y.; Zheng, B.-J.; Wang, X.; Zhang, L. Potent Neutralization of Mers-Cov by Human Neutralizing Monoclonal Antibodies to the Viral Spike Glycoprotein. *Sci. Transl. Med.* **2014**, *6* (234), 234ra259.
(23) Casalino, L.; Gaieb, Z.; Goldsmith, J. A.; Hjorth, C. K.; Dommer, A. C.; Harbison, A. M.; Fogarty, C. A.; Barros, E. P.; Taylor, B. C.; McLellan, J. S.; Fadda, E.; Amaro, R. E. Beyond Shielding: The Roles of Glycans in the Sars-Cov-2 Spike Protein. *ACS Cent. Sci.* **2020**, *6* (10), 1722−1734.
(24) Jones, B. E.; Brown-Augsburger, P. L.; Corbett, K. S.; Westendorf, K.; Davies, J.; Cujec, T. P.; Wiethoff, C. M.; Blackbourne, J. L.; Heinz, B. A.; Foster, D.; Higgs, R. E.; Balasubramaniam, D.; Wang, L.; Zhang, Y.; Yang, E. S.; Bidshahri, R.; Kraft, L.; Hwang, Y.; Žentelis, S.; Jepson, K. R.; Goya, R.; Smith, M. A.; Collins, D. W.; Hinshaw, S. J.; Tycho, S. A.; Pellacani, D.; Xiang, P.; Muthuraman, K.; Sobhanifar, S.; Piper, M. H.; Triana, F. J.; Hendle, J.; Pustilnik, A.; Adams, A. C.; Berens, S. J.; Baric, R. S.; Martinez, D. R.; Cross, R. W.; Geisbert, T. W.; Borisevich, V.; Abiona, O.; Belli, H. M.; de Vries, M.; Mohamed, A.; Dittmann, M.; Samanovic, M. I.; Mulligan, M. J.; Goldsmith, J. A.; Hsieh, C. L.; Johnson, N. V.; Wrapp, D.; McLellan, J. S.; Barnhart, B. C.; Graham, B. S.; Mascola, J. R.; Hansen, C. L.; Falconer, E. The Neutralizing Antibody, Ly-Cov555, Protects against Sars-Cov-2 Infection in Nonhuman Primates. *Sci. Transl. Med.* **2021**, *13* (593), abf1906.
(25) Hansen, J.; Baum, A.; Pascal, K. E.; Russo, V.; Giordano, S.; Wloga, E.; Fulton, B. O.; Yan, Y.; Koon, K.; Patel, K.; Chung, K. M.; Hermann, A.; Ullman, E.; Cruz, J.; Rafique, A.; Huang, T.; Fairhurst, J.; Libertiny, C.; Malbec, M.; Lee, W. Y.; Welsh, R.; Farr, G.; Pennington, S.; Deshpande, D.; Cheng, J.; Watty, A.; Bouffard, P.; Babb, R.; Levenkova, N.; Chen, C.; Zhang, B.; Romero Hernandez, A.; Saotome, K.; Zhou, Y.; Franklin, M.; Sivapalasingam, S.; Lye, D. C.; Weston, S.; Logue, J.; Haupt, R.; Frieman, M.; Chen, G.; Olson, W.; Murphy, A. J.; Stahl, N.; Yancopoulos, G. D.; Kyratsous, C. A. Studies in Humanized Mice and Convalescent Humans Yield a Sars-Cov-2 Antibody Cocktail. *Science* **2020**, *369* (6506), 1010−1014.
(26) Tortorici, M. A.; Czudnochowski, N.; Starr, T. N.; Marzi, R.; Walls, A. C.; Zatta, F.; Bowen, J. E.; Jaconi, S.; Di Iulio, J.; Wang, Z.; De Marco, A.; Zepeda, S. K.; Pinto, D.; Liu, Z.; Beltramello, M.; Bartha, I.; Housley, M. P.; Lempp, F. A.; Rosen, L. E.; Dellota, E., Jr.; Kaiser, H.; Montiel-Ruiz, M.; Zhou, J.; Addetia, A.; Guarino, B.; Culap, K.; Sprugasci, N.; Saliba, C.; Vetti, E.; Giacchetto-Sasselli, I.; Fregni, C. S.; Abdelnabi, R.; Foo, S. C.; Havenar-Daughton, C.; Schmid, M. A.; Benigni, F.; Cameroni, E.; Neyts, J.; Telenti, A.; Virgin, H. W.; Whelan, S. P. J.; Snell, G.; Bloom, J. D.; Corti, D.; Veesler, D.; Pizzuto, M. S. Broad Sarbecovirus Neutralization by a Human Monoclonal Antibody. *Nature* **2021**, *597* (7874), 103−108.
(27) Monteil, V.; Kwon, H.; Prado, P.; Hagelkrüys, A.; Wimmer, R. A.; Stahl, M.; Leopoldi, A.; Garreta, E.; Hurtado Del Pozo, C.; Prosper, F.; Romero, J. P.; Wirnsberger, G.; Zhang, H.; Slutsky, A. S.; Conder, R.; Montserrat, N.; Mirazimi, A.; Penninger, J. M. Inhibition of Sars-Cov-2 Infections in Engineered Human Tissues Using Clinical-Grade Soluble Human Ace2. *Cell* **2020**, *181* (4), 905−913.
(28) Chan, K. K.; Dorosky, D.; Sharma, P.; Abbasi, S. A.; Dye, J. M.; Kranz, D. M.; Herbert, A. S.; Procko, E. Engineering Human Ace2 to Optimize Binding to the Spike Protein of Sars Coronavirus 2. *Science* **2020**, *369* (6508), 1261−1265.
(29) Huang, X.; Pearce, R.; Zhang, Y. De Novo Design of Protein Peptides to Block Association of the Sars-Cov-2 Spike Protein with Human Ace2. *Aging* **2020**, *12* (12), 11263−11276.
(30) Ju, B.; Zhang, Q.; Ge, J.; Wang, R.; Sun, J.; Ge, X.; Yu, J.; Shan, S.; Zhou, B.; Song, S.; Tang, X.; Yu, J.; Lan, J.; Yuan, J.; Wang, H.; Zhao, J.; Zhang, S.; Wang, Y.; Shi, X.; Liu, L.; Zhao, J.; Wang, X.; Zhang, Z.; Zhang, L. Human Neutralizing Antibodies Elicited by Sars-Cov-2 Infection. *Nature* **2020**, *584* (7819), 115−119.
(31) Zhou, D.; Duyvesteyn, H. M. E.; Chen, C. P.; Huang, C. G.; Chen, T. H.; Shih, S. R.; Lin, Y. C.; Cheng, C. Y.; Cheng, S. H.; Huang, Y. C.; Lin, T. Y.; Ma, C.; Huo, J.; Carrique, L.; Malinauskas, T.; Ruza, R. R.; Shah, P. N. M.; Tan, T. K.; Rijal, P.; Donat, R. F.; Godwin, K.; Buttigieg, K. R.; Tree, J. A.; Radecke, J.; Paterson, N. G.; Supasa, P.; Mongkolsapaya, J.; Screaton, G. R.; Carroll, M. W.; Gilbert-Jaramillo, J.; Knight, M. L.; James, W.; Owens, R. J.; Naismith, J. H.; Townsend, A. R.; Fry, E. E.; Zhao, Y.; Ren, J.; Stuart, D. I.; Huang, K. A. Structural Basis for the Neutralization of Sars-Cov-2 by an Antibody from a Convalescent Patient. *Nat. Struct. Mol. Biol.* **2020**, *27* (10), 950−958.
(32) Cao, L.; Goreshnik, I.; Coventry, B.; Case, J. B.; Miller, L.; Kozodoy, L.; Chen, R. E.; Carter, L.; Walls, A. C.; Park, Y. J.; Strauch, E. M.; Stewart, L.; Diamond, M. S.; Veesler, D.; Baker, D. De Novo Design of Picomolar Sars-Cov-2 miniprotein Inhibitors. *Science* **2020**, *370* (6515), 426−431.
(33) Starr, T. N.; Greaney, A. J.; Hilton, S. K.; Ellis, D.; Crawford, K. H. D.; Dingens, A. S.; Navarro, M. J.; Bowen, J. E.; Tortorici, M. A.; Walls, A. C.; King, N. P.; Veesler, D.; Bloom, J. D. Deep Mutational Scanning of Sars-Cov-2 Receptor Binding Domain Reveals Constraints on Folding and Ace2 Binding. *Cell* **2020**, *182* (5), 1295−1310.
(34) Hunt, A. C.; Case, J. B.; Park, Y. J.; Cao, L.; Wu, K.; Walls, A. C.; Liu, Z.; Bowen, J. E.; Yeh, H. W.; Saini, S.; Helms, L.; Zhao, Y. T.; Hsiang, T. Y.; Starr, T. N.; Goreshnik, I.; Kozodoy, L.; Carter, L.; Ravichandran, R.; Green, L. B.; Matochko, W. L.; Thomson, C. A.; Vögeli, B.; Krüger, A.; VanBlargan, L. A.; Chen, R. E.; Ying, B.; Bailey, A. L.; Kafai, N. M.; Boyken, S. E.; Ljubetič, A.; Edman, N.; Ueda, G.; Chow, C. M.; Johnson, M.; Addetia, A.; Navarro, M. J.; Panpradist, N.; Gale, M., Jr.; Freedman, B. S.; Bloom, J. D.; Ruohola-Baker, H.; Whelan, S. P. J.; Stewart, L.; Diamond, M. S.; Veesler, D.; Jewett, M. C.; Baker, D. Multivalent Designed Proteins Neutralize Sars-Cov-2 Variants of Concern and Confer Protection against Infection in Mice. *Sci. Transl. Med.* **2022**, *14* (646), eabn1252.
(35) Greaney, A. J.; Starr, T. N.; Barnes, C. O.; Weisblum, Y.; Schmidt, F.; Caskey, M.; Gaebler, C.; Cho, A.; Agudelo, M.; Finkin, S.; Wang, Z.; Poston, D.; Muecksch, F.; Hatziioannou, T.; Bieniasz, P. D.; Robbiani, D. F.; Nussenzweig, M. C.; Bjorkman, P. J.; Bloom, J. D. Mapping Mutations to the Sars-Cov-2 Rbd That Escape Binding by Different Classes of Antibodies. *Nat. Commun.* **2021**, *12* (1), 4196.

https://doi.org/10.1021/acs.jcim.2c00500
J. Chem. Inf. Model. 2022, 62, 3618−3626